Applied Catalysis B: Environmental 125 (2012) 149–157

Contents lists available at SciVerse ScienceDirect

Applied Catalysis B: Environmental

journal homepage: www.elsevier.com/locate/apcatb

Stoichiometric and non-stoichiometric perovskite-based catalysts: Consequences on surface properties and on catalytic performances in the decomposition of N_2O from nitric acid plants

Y. Wu, X. Ni, A. Beaurain, C. Dujardin*, P. Granger

Univ Lille Nord de France, Unité de Catalyse et de Chimie du Solide–UCCS, CNRS UMR 8181, USTL, Cité Scientifique, Bâtiment C3, 59655, Villeneuve d'Ascq, France

ARTICLE INFO

Article history:
Received 15 February 2012
Received in revised form 11 May 2012
Accepted 24 May 2012
Available online 4 June 2012

Keywords:
Perovskite
$LaCoO_3$
N_2O decomposition
High temperature resistance
XPS

ABSTRACT

Catalytic activity for the N_2O decomposition into N_2 was investigated on perovskite-based materials in the presence of 5 vol% NO, 6 vol% O_2 and 15 vol% H_2O. This feed is typical of industrial conditions for nitric acid plants operating at high temperature (850–900 °C). The catalytic properties were found to be sensitive to the surface composition as revealed by XRD and XPS. Surface reconstructions on La and Co deficient perovskites induced surface La or Co enrichment. The latter governed the catalytic properties at medium and high temperature and was related to change in oxygen mobility. The presence of water was found as an outstanding parameter to speed up structural changes at the surface. However the presence of water had globally a negative impact in the catalytic activity in N_2O decomposition. Surface changes which determined the extent of deactivation were more accentuated on Co-deficient perovskites due to La_2O_3 segregation. Higher resistance to deactivation was obtained on La-deficient perovskites such as $La_{0.8}CoO_3$ and $La_{0.9}Co_{0.8}Fe_{0.2}O_3$. Surface reconstruction was evidenced at high temperature in severe reaction conditions.

1. Introduction

There is a growing interest to minimize the emissions of nitrous oxide (N_2O) as side-product from nitric acid plants. Nitrous oxide has a global warming potential of approximately 310 times higher than that of CO_2 [1,2]. Different strategies are already implemented at industrial scale but they are still suffering from significant drawbacks. The latter are essentially associated with a poor selectivity and sometimes a short lifetime in particular when the catalytic process is inserted in the ammonia burner. Bulk or supported mixed metal oxides and metal-loaded zeolites are developed for catalytic N_2O decomposition in nitric acid plants (Co_2AlO_4/CeO_2 by Yara International, CuO/Al_2O_3 by BASF, $La_{0.8}Ce_{0.2}CoO_3$ by Johnson Matthey and FeZSM-5 by Uhde) [1]. Recently alternative catalytic formulations were evaluated under model reaction mixture for N_2O decomposition, such as yttrium-doped zirconia [3], ceria-zirconia [4], $AB_{1-x}B'_xO_3$ perovskites with A = La or Ca, B = Mn or Fe, and B' = Cu or Ni [5], metal-substituted hexaaluminates [6], Fe_2O_3/Al_2O_3 [7] and mayenite [8].

Previous *in situ* XRD measurements performed in our laboratory in wet atmosphere (3 vol% H_2O) at high temperature revealed the excellent thermal stability of perovskite based catalysts. This makes them suitable materials for high temperature applications especially the decomposition of nitrous oxides from nitric acid plants [9]. However, the influence of the surface composition and subsequent surface reconstructions related to the segregation of lanthanum and cobalt oxide Co_3O_4 are not clearly elucidated even though they can significantly alter the catalytic properties of $LaCoO_3$ in the decomposition of nitrous oxide. Indeed, X-ray photoelectron spectroscopy measurements usually highlight a surface atomic ratio of Co/La <1 thus reflecting a surface enrichment in lanthanum [10,11].

A possible support effect related to the presence of segregated amorphous phase at the surface of perovskite can either promote or inhibit the activity of the active phase during the catalytic decomposition of N_2O at high temperature. Higher catalytic performances are expected in the case of more crystalline surface despite the strong decrease of specific surface area. Another possibility is the segregation of lanthanum or cobalt oxide at the surface of perovskite which induces a strong support interaction. Moreover the segregation can also have a promoting/inhibiting effect towards the catalytic decomposition of nitrous oxide.

Non-stoichiometric perovskite-based catalysts have been examined in this study. The aim was to investigate induced effects of segregated oxides on perovskite with regard to the catalytic properties. Moreover, an additional aspect of practical interest was

* Corresponding author. Tel.: +33 328 778 529; fax: +33 320 436 561.
E-mail address: christophe.dujardin@univ-lille1.fr (C. Dujardin).

0926-3373/$ – see front matter © 2012 Elsevier B.V. All rights reserved.
http://dx.doi.org/10.1016/j.apcatb.2012.05.033

taken into account since no NO decomposition should occur to preserve the cost-efficiency of those typical industrial plants. To that end, the catalyst selectivity of high temperature N_2O abatement process was studied.

2. Experimental

Three series of stoichiometric and non-stoichiometric perovskite-based catalysts ($LaCo_{1-y}O_3$ $La_{1-x}CoO_3$ and $La_{1-x}Co_{0.8}Fe_{0.2}O_3$) were synthesized according to a conventional sol–gel method involving a citrate route [12]. Precursors thus obtained were dried overnight at 80 °C and then calcined in air at 600 °C or 900 °C for 8 h.

Specific surface areas were determined by N_2 physisorption at 77 K with Quantasorb Quantachrome device with suitable weight for low specific area materials. Powder X-ray diffraction (XRD) was performed at room temperature (RT) using a Bruker AXS D8 Advance diffractometer working in Bragg–Brentano geometry and equipped with a LynxEye Super Speed detector. Data were collected with Cu Kα ($\lambda = 0.154$ nm) in the 10–100° 2θ range with a 0.02° 2θ step. The Fullprof Suite program [13] was used for Rietveld refinement. The Thompson-Cox-Hastings pseudo-Voigt function was chosen for the peak profiles. LaB_6 was used as standard to derive the instrument resolution. An isotropic size parameter of Gaussian character was refined to take into account the contribution of sample in the broadening of Bragg peaks.

XPS experiments were performed using an AXIS Ultra DLD Kratos spectrometer equipped with a monochromatised aluminium source (150 W) and charge compensation gun. The analyzer was operated in a constant pass energy mode ($E_{pass} = 40$ eV). All binding energies were referenced to the C 1s core level at 285 eV. The peak areas were estimated after subtracting backgrounds according to the procedure suggested by Shirley [14]. A special attention was required for the estimate of surface atomic Co/La and Fe/La ratios after the subtraction of the Auger contributions from Fe and Co respectively.

H_2-temperature-programmed reduction experiments (H_2-TPR) were carried out in a Micromeritics Autochem II 2920 with 5 vol% H_2 in Ar and a gradual heating rate of 5 °C/min.

Catalytic decomposition of N_2O was studied in a fixed-bed flow reactor in temperature-programmed conditions (20–900 °C, 2 °C/min) using 0.7 g of catalyst. The total flow rate was adjusted to 15 L h^{-1} in order to get a gas hourly space velocity of approximately 30,000 h^{-1}. The reactant mixture was composed of 0.1 vol% N_2O, 5 vol% NO, 6 vol% O_2, 15 vol% H_2O and balanced by He. A second catalytic test was performed after ageing overnight at 900 °C under reactant mixture (labeled as ageing procedure) in order to characterize the stability of our catalysts. The concentration of N_2O was followed with a dispersive IR analyser for N_2O detection (Emerson XStream). Part of effluents was then diluted eleven-fold by means of mass flow controllers before quantification of NO and NO_2 with a NO_x analyzer (Thermo 42i-HL) using chemiluminescence detection. N_2O conversion was calculated according to equation (1) with $F_{N_2O,\,inlet}$ and $F_{N_2O,\,outlet}$ standing for respectively inlet and outlet molar flow of N_2O.

$$X_{N_2O} = \frac{F_{N_2O,\,inlet} - F_{N_2O,\,outlet}}{F_{N_2O,\,inlet}} \quad (1)$$

3. Results and discussion

3.1. Evaluation of catalytic properties from temperature-programmed experiments

The catalytic activity for the N_2O decomposition into N_2 has been evaluated in the presence of 5 vol% NO, 6 vol% O_2 and 15 vol% H_2O. This feed is a typical composition of a gas leaving industrial ammonia burner from nitric acid plants operating at high temperature. It is worthwhile to note that, up to now, most of the catalytic testings earlier reported in the literature were achieved at lab-scale far from real exhaust gas composition [1,4]. For example, low NO_x concentration can be considered as favourable conditions. Moreover at high temperature operating conditions, NO_x conversion must be avoided to preserve high yields of nitric acid. In our operating conditions, it was found that no NO conversion occurs above 600 °C for all tested samples. This emphasizes the high selectivity of perovskite-based materials for such type of application thus opening practical interests. Below that temperature, significant oxidation of NO to NO_2 takes places (results not shown). The conversion of N_2O usually starts significantly above 500 °C when the production of NO_2 becomes thermodynamically unfavoured. Furthermore the desorption/decomposition of those ad-NO_x species takes place as reported elsewhere [15]. Fig. 1 compares temperature programmed-conversion curves recorded for the decomposition of N_2O on calcined samples (A) and on overnight aged catalysts (B). Qualitative comparisons can be achieved by examining the shift observed on the light-off curves towards higher temperature which highlights a detrimental effect on the catalytic performance. Based on such comparisons, a beneficial effect of Fe incorporation is discernible on calcined stoichiometric samples whereas the reverse tendency seems to be observed on La-deficient based perovskites. This detrimental effect accentuates with a gradual decrease in La concentration on fresh catalyst.

Additional information can be further related to changes in surface properties. Arrhenius plots were calculated from N_2O conversion obtained during temperature-programmed experiments on catalysts calcined at 600 °C or 900 °C firstly (Fig. 2a) and on the same catalysts aged overnight under reaction conditions at 900 °C secondly (Fig. 2b). Activation energy values reported in Table 1 have been calculated from the slope of the Arrhenius plots. Rate constants calculated from Eq. (2) were used where W stands for the mass of catalyst, Q_0 the total flow rate and k the rate constant. Eq. (2) is established for a plug flow reactor and takes into account a first order kinetic reaction for N_2O decomposition as reported elsewhere [19] and also verified in this study on $LaCoO_3$. TPR conversions (X_{N_2O}) considered in these calculations were in the range 4–12%.

$$k = \frac{Q_0}{W} \ln\left(\frac{1}{1 - X_{N_2O}}\right) \quad (2)$$

The specific reaction rate was calculated according to Eq. (3). $F_{N_2O,\,inlet}$ stands for the molar flow rate for N_2O at the inlet of the reactor.

$$r = k\frac{F_{N_2O,\,inlet}(1 - X_{N_2O})}{Q_0} \quad (3)$$

Internal diffusion should not occur significantly in this conversion range according to the estimate of the effectiveness factor η in our experimental conditions. The effectiveness factor η was estimated based on the calculation of the Weitz modulus given by Eq. (4). This corresponds to the modified criteria $\phi^2\eta$ related to none isothermal reactions and taking into account any apparent reaction order values.

$$\phi^2\eta = R^2\frac{r\rho_p}{CD_e} \quad (4)$$

R represents the radius of the grain $\sim 7.5 \times 10^{-5}$ m, r the specific reaction rate at 600 °C, ρ_p the catalyst density (6.4×10^5 g m^{-3}), C the inlet concentration of gaseous N_2O (0.04 mol m^{-3}), D_e the effective diffusion coefficient ($\sim 1.1 \times 10^{-4}$ m^2 s^{-1}) in a Knudsen regime [16]. The estimates for the Weisz modulus ϕ remained very low ($\sim 1.2 \times 10^{-5}$) and corresponded to numerical solutions for η

Table 1
Catalytic performances of $La_{1-x}Co_{1-y}O_3$ and $La_{1-x}Co_{0.8}Fe_{0.2}O_3$ solids in N_2O decomposition.

Theoretical composition	$T_{calcination}$ (°C)	T_{50}[a] (°C)		Apparent activation energy (kJ/mol)		Specific reaction rate (mol s^{-1} g^{-1})[b]		Intrinsic reaction rate (mol s^{-1} m^{-2})[b]	
		Calcined	Aged	Calcined	Aged	Calcined	Aged	Calcined	Aged
$LaCoO_3$	600 °C	570	642	162	164	3.7×10^{-8}	2.5×10^{-8}	2.5×10^{-9}	1.2×10^{-8}
$LaCoO_3$	900 °C	580	642	142	168	3.3×10^{-8}	2.3×10^{-8}	7.1×10^{-9}	0.8×10^{-8}
$LaCo_{0.8}O_3$	900 °C	596	673	145	167	1.9×10^{-8}	1.0×10^{-8}	1.6×10^{-9}	0.7×10^{-8}
$La_{0.8}CoO_3$	900 °C	588	625	195	177	2.0×10^{-8}	3.8×10^{-8}	8.4×10^{-9}	2.4×10^{-8}
$LaCo_{0.8}Fe_{0.2}O_3$	900 °C	563	648	170	153	4.3×10^{-8}	2.5×10^{-8}	9.6×10^{-9}	0.9×10^{-8}
$La_{0.9}Co_{0.8}Fe_{0.2}O_3$	900 °C	588	622	178	167	2.4×10^{-8}	3.9×10^{-8}	9.4×10^{-9}	2.1×10^{-8}
$La_{0.8}Co_{0.8}Fe_{0.2}O_3$	900 °C	599	649	245	184	1.1×10^{-8}	2.3×10^{-8}	5.2×10^{-9}	1.4×10^{-8}

[a] Temperature corresponding to 50% N_2O conversion.
[b] Measured at 535 °C for calcined catalyst and 575 °C for aged catalyst.

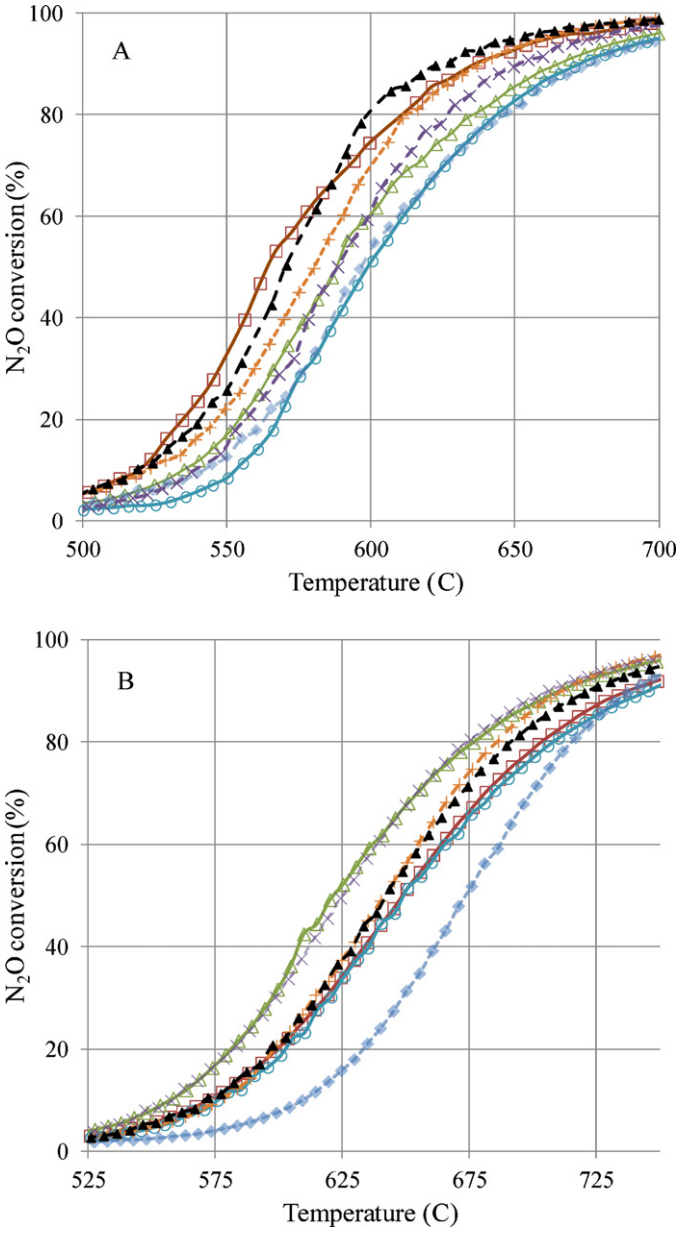

Fig. 1. Comparison of N_2O conversion during the temperature-programmed reaction under He+0.1% N_2O+5% NO+6% O_2+15% H_2O of calcined sample (a) at 600 °C: $LaCoO_3$ (▲) and at 900 °C: $LaCoO_3$ (+), $LaCo_{0.8}O_3$ (♦), $La_{0.8}CoO_3$ (*x*), $LaCo_{0.8}Fe_{0.2}O_3$ (□), $La_{0.9}Co_{0.8}Fe_{0.2}O_3$ (Δ) and $La_{0.8}Co_{0.8}Fe_{0.2}O_3$ (○) and after ageing thermal treatment at 900 °C (b).

very close to the unity. The occurrence of heat transfer was also evaluated on the basis of the calculation of the Prater number $\beta_1 \sim 2.2 \times 10^{-5}$ taking into account a thermal conductivity coefficient λ_e of approximately 17.0 W m^{-1} K^{-1} [17]. Accordingly, the maximum deviation in temperature between the core and the surface of the grain should not exceed 0.02 °C in this present study [18]. Based on these calculations, the estimates of the apparent activation energy collected in Table 1 are of the same order of magnitude than

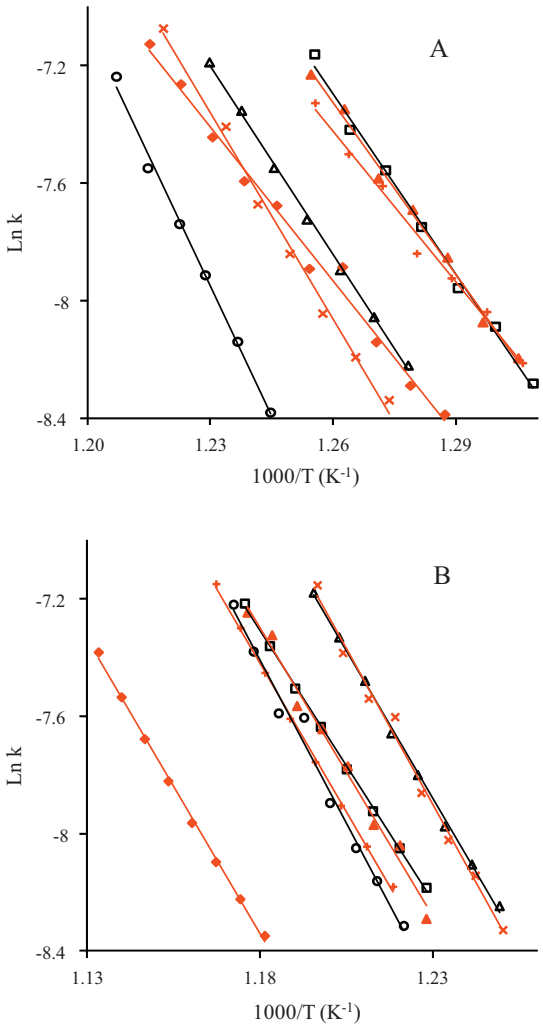

Fig. 2. Arrhenius plot over the N_2O conversion range from 4% to 12% during the temperature-programmed reaction under He+0.1% N_2O+5% NO+6% O_2+15% H_2O of calcined sample (a) at 600 °C: $LaCoO_3$ (▲) and at 900 °C: $LaCoO_3$ (+), $LaCo_{0.8}O_3$ (♦), $La_{0.8}CoO_3$ (*x*), $LaCo_{0.8}Fe_{0.2}O_3$ (□), $La_{0.9}Co_{0.8}Fe_{0.2}O_3$ (Δ) and $La_{0.8}Co_{0.8}Fe_{0.2}O_3$ (○) and after ageing thermal treatment at 900 °C (b).

those already reported over mixed oxides [19]. This trend underlines the absence of significant external diffusion. Furthermore it emphasizes the fact that these measurements were achieved in chemical regimes with the absence of significant heat and mass transfer phenomena. Specific rates calculated on freshly-prepared catalysts at 535 °C and aged samples at 575 °C reported in Table 1 are also compared. The specific reaction rate values are smaller than that obtained under He + N_2O reported by Kondratenko et al. [20] or Perez-Alonso et al. [21]. Strong inhibition by O_2, NO and H_2O can explain the smaller values obtained in the present study. At low temperature, it was earlier found that the stabilisation of strongly chemisorbed nitrate species likely block the oxygen mobility and subsequent N_2O decomposition [22]. This effect has been verified on $LaCoO_3$ calcined at 900 °C from steady state kinetics measurements at 490 °C (conversion 2–5%). A negative apparent order with respect to the partial pressure of NO, O_2 and H_2O of approximately −0.2, −0.2 and −0.5 was thus highlighted.

More obvious comparisons can be obtained from the intrinsic rate values expressed per m^2 which led to the highest value on $La_{0.8}CoO_3$ calcined at 900 °C. The decrease of intrinsic reaction rate after ageing was less significant on $La_{0.8}CoO_3$ than on aged $LaCoO_3$ and $LaCo_{0.8}O_3$.

Parallel to these observations significant deviations are observable on the apparent activation energy with a significant decrease on $La_{0.8}CoO_3$ after ageing whereas the reverse trend is seen for $LaCoO_3$ and $LaCo_{0.8}O_3$.

Interestingly, a beneficial effect of Fe incorporation was only noticeable on stoichiometric samples whereas the reverse tendency was observed on La-deficient based perovskites. As observed, the detrimental effect accentuates with a gradual decrease in La content.

Possible segregation of cobalt on calcined $La_{0.8}CoO_3$ and $La_{0.8}Co_{0.8}Fe_{0.2}O_3$ was related to a drastic increase in the apparent activation energy of the calcined samples. After ageing, deactivation of all the catalysts was observed with a shift of light-off curves towards higher temperature. Specific and intrinsic activities also decreased while a decrease in E_{app} was observed highlighting a compensation effect except on La-enriched samples. The decrease in E_{app} was less accentuated on $La_{0.8}CoO_3$ and on $La_{0.9}Co_{0.8}Fe_{0.2}O_3$ which underlines a slower deactivation.

Deactivation led to a significant loss of activity but the reactivity sequence previously established on the calcined samples differed from that obtained on aged samples. Clearly the highest intrinsic activity was observed on $La_{0.8}CoO_3$. Further iron incorporation provided synergy effects on specific reaction rate. On the contrary, a slight detrimental effect was discernible when examining the specific and intrinsic rates on $La_{0.8}Co_{0.8}Fe_{0.2}O_3$ even if a decrease in the apparent activation energy was noticeable. This effect is attenuated on $La_{0.9}Co_{0.8}Fe_{0.2}O_3$ but still persists in lower extent with the same trend on E_{app}. Hence, remarkable catalytic activities were shown for $La_{0.8}CoO_3$ and $La_{0.9}Co_{0.8}Fe_{0.2}O_3$ after an ageing procedure. Specific surface composition could be expected for slightly La-deficient perovskites.

3.2. Deactivation during long term catalytic measurements

Catalytic activity was followed after ageing procedure during 3 days under reaction mixture on $LaCo_{0.8}Fe_{0.2}O_3$ and on $La_{0.9}Co_{0.8}Fe_{0.2}O_3$. The temperature profile is presented in Fig. 3. N_2O conversion was complete during ageing procedure at 900 °C on both samples. For a better assessment of the stability, the N_2O conversion was compared at 632 °C in order to evaluate the extent of deactivation during a long term ageing at 900 °C. After overnight ageing, the reconstruction of the surface was supposed to be almost complete. The N_2O conversion at 632 °C is 54% after overnight ageing and 43% after the additional 3 days of ageing

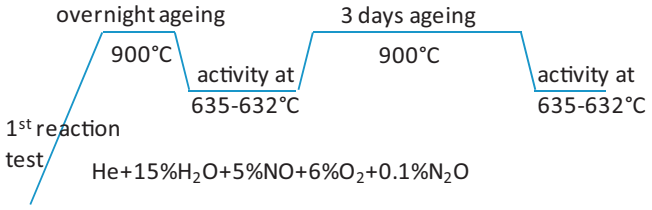

Fig. 3. Temperature profile used for the stability tests of catalytic performances on $La_{0.9}Co_{0.8}Fe_{0.2}O_3$.

on $La_{0.9}Co_{0.8}Fe_{0.2}O_3$. The change of temperature to balance the decrease of N_2O conversion was calculated with the apparent activation energy previously estimated on aged catalyst. In order to reach the same conversion (54%), the temperature should be increased from 632 °C to 641 °C which corresponds to a shift of 9 °C. Previous shift of temperature observed during first ageing procedure was 34 °C (Table 1). The decrease of deactivation from 34 °C to 9 °C clearly underlined the stabilisation of catalytic properties in reaction conditions. Obviously, the deactivation of catalysts took place in the first few hours in reaction conditions. Then the stabilisation of catalytic properties was obtained. The complete N_2O catalytic conversion around 900 °C was then expected to be maintained for a long time in such severe conditions.

A similar procedure was performed on stoichiometric $LaCo_{0.8}Fe_{0.2}O_3$ and the N_2O conversion at 635 °C were respectively 45% after overnight ageing and 37% after the additional 3 days ageing. The lower conversion level is in agreement with previous catalytic measurements. The calculation of corresponding ΔT to reach 45% conversion is 9 °C after 3 days ageing when determined with previously calculated apparent activation energy. This value is smaller than that obtained during the first ageing procedure (85 °C, Table 1) underlining the progressive stabilisation of perovskite. Clearly, the lower lanthanum content between $LaCo_{0.8}Fe_{0.2}O_3$ and $La_{0.9}Co_{0.8}Fe_{0.2}O_3$ prevents the deactivation of catalytic performances at high temperature in reaction conditions.

3.3. Surface and bulk properties of stoichiometric $LaCoO_3$ solids

XRD patterns recorded on the $LaCoO_3$ solids put into evidence the rhombohedral perovskite structure for both calcination temperatures (Fig. 4A and B, XRD patterns (a) currently identified by the appearance of a doublet at $2\theta = 32.8–33.2°$ on the main X-ray lines. An increase of calcination temperature to 900 °C led to an increase of the crystallite size associated to a sharp decrease of the specific surface area from 15 m^2/g to 4.6 m^2/g (Table 2). Such structural features are of great importance for high temperature catalytic applications since intrafacial mechanism involving oxygen lattice usually prevails. In this present study the oxygen mobility and related formation of oxygen defects would govern the catalytic properties in N_2O decomposition as earlier discussed [9]. Accordingly, Royer et al. [23] suggested a simple model for depicting the morphology of perovskites and the formation of agglomerates concluding that the oxygen mobility is enhanced on the small crystallites. However, it was earlier stated that oxygen availability is also facilitated by a faster diffusion process along the grain boundaries. A rough estimation of theoretical surface S_{th} from the crystallite size in Table 2 can be compared with the BET surface S_{BET} calculated from nitrogen physisorption. The S_{th}/S_{BET} ratio corresponds to the fraction of surface lost by agglomeration between crystal domains as earlier explained [24]. Variations observed on S_{th}/S_{BET} ratio reported in Table 2 essentially show that the loss of specific surface area with a raise in calcination temperature is due to the growth of the perovskite crystallites. Similar trend takes place when calcined $LaCoO_3$ at 600 °C is aged under

Table 2
Structural and textural properties of $La_{1-x}CoO_3$, $LaCo_{1-y}O_3$ and $La_{1-x}Co_{0.8}Fe_{0.2}O_3$ solids.

Theoretical composition	$T_{calcination}$ (°C)	Structure[a]		S_{BET} ($m^2\ g^{-1}$)		Crystallite size (nm)		S_{th} ($m^2\ g^{-1}$)[b]		S_{th}/S_{BET}	
		Calcined	Aged	Calcined	Aged	Calcined	Aged	Calcined	Aged	Calcined	Aged
$LaCoO_3$	600 °C	R	R	15	2.0	14.4	94.5	57.2	8.7	3.8	4.4
	900 °C	R	R	4.6	2.8	63.2	104.6	13.0	7.9	2.8	2.8
$LaCo_{0.8}O_3$	600 °C	$R+La_2O_3$	–	18.7	–	11.2	–	73.5	–	3.9	–
	900 °C	$R+La_2O_3$	$R+La(OH)_3$	11.9	1.3	34.1	44.2	24.1	18.6	2.0	14.3
$LaCo_{0.6}O_3$	600 °C	$R+La_2O_3$	–	21.2	–	6.5	–	126.6	–	6.0	–
$La_{0.8}CoO_3$	900 °C	$R+Co_3O_4$	$R+Co_3O_4+CoO$	2.4	1.6	119.5	132.9	6.9	6.2	2.9	3.9
$LaCo_{0.8}Fe_{0.2}O_3$	900 °C	R	R	4.5	2.7	67.0	55.5	12.3	14.8	2.7	5.5
$La_{0.9}Co_{0.8}Fe_{0.2}O_3$	900 °C	$R+Co_3O_4$	R	2.5	1.9	98.5	94.4	8.4	8.7	3.3	4.6
$La_{0.8}Co_{0.8}Fe_{0.2}O_3$	900 °C	$R+Co_3O_4$	$R+Co_3O_4+CoO$	2.2	1.6	72.4	70.9	11.4	11.6	5.2	7.3

[a] R: rhombohedral perovskite phase.
[b] S_{th}, specific surface area calculated assuming cubic particles of size D_p (crystallite size from Rietveld refinement) and a density (ρ) of $LaCoO_3$ equal to 7.29 g/cm^3; $S_{th} = 6/(\rho \cdot D_p)$.

reactive conditions at 900 °C in wet atmosphere with a significant increase in the crystal size domain. These results underline the decrease of catalytic performances when sintering occurs during reaction or after calcination at high temperature.

The reducibility of Co based species has been examined from H_2-temperature-programmed reduction experiments. Such experiments usually highlight the mobility and the reactivity of surface and bulk oxygen species from the perovskite ascribed to the strength of the Co—O bond depending on the chemical environment. Clearly, the reducibility of $LaCoO_3$ is influenced by the calcination temperature (Fig. 5). The typical profile related to H_2 consumption exhibits two temperature domains corresponding to the reduction of Co^{3+} into Co^{2+} around 250–450 °C and the subsequent reduction of Co^{2+} into Co^0 above 500 °C. This two-steps reduction process is in agreement with the values calculated for the atomic H/Co ratio from H_2 uptakes of respectively ~1 and ~2 according to the margin of error [9]. As observed, the maximum of both reduction peaks of $LaCoO_3$ is shifted to higher temperature when the perovskite is calcined at 900 °C. This is in agreement with previous observations reported by Royer et al. [24]. The latter underlined a densification with an increase in calcination temperature which induces a lowering of the free surface between the crystallites. However, in our case the crystallite growth after calcination at 900 °C is likely the most significant property associated to a higher resistance to diffusion on larger crystallites further explaining the shift of the reduction processes to higher temperature.

In parallel to modifications in structural properties according to the calcination temperature, significant changes in surface composition might take place as illustrated by Chiarello et al. [25]. These authors observed the preservation of the perovskite $LaCoO_3$

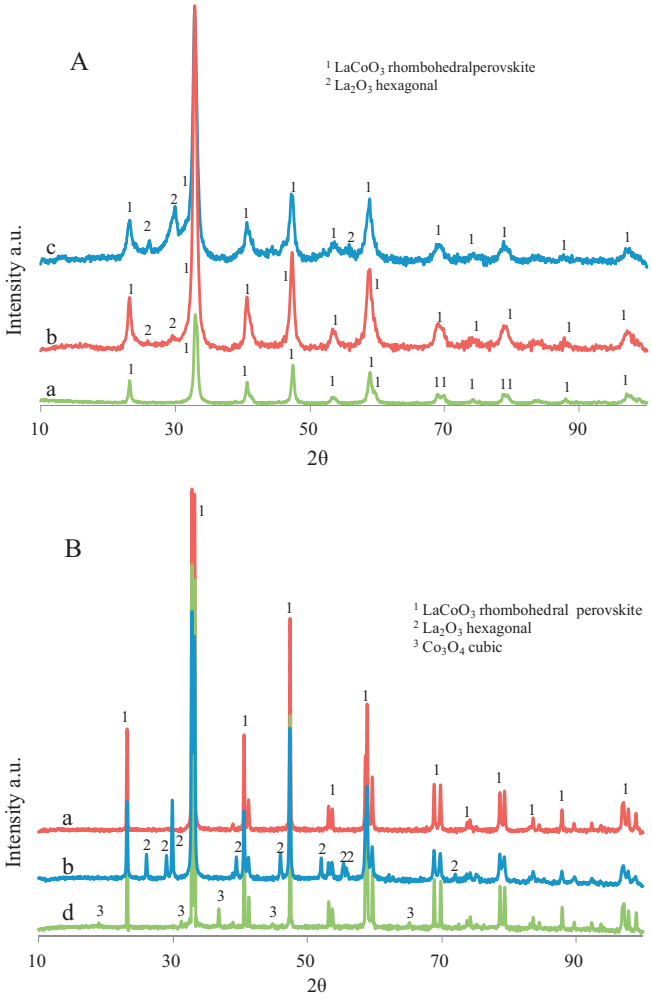

Fig. 4. XRD pattern of $LaCoO_3$ (a), $LaCo_{0.8}O_3$ (b), $LaCo_{0.6}O_3$ (c) and $La_{0.8}CoO_3$ (d) samples after calcination at 600 °C (A) or 900 °C (B).

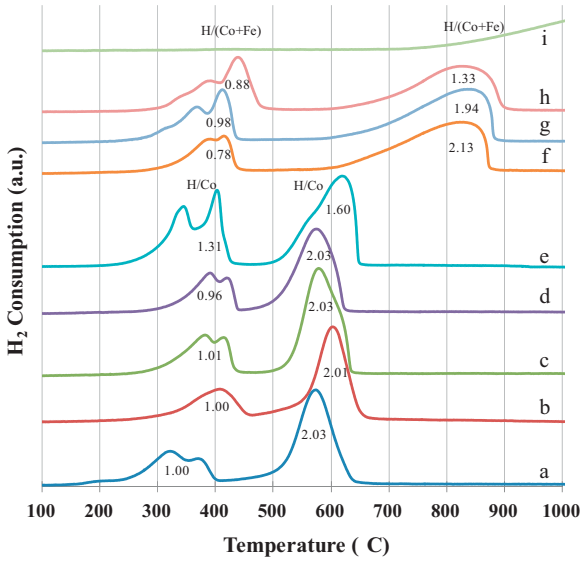

Fig. 5. H_2-TPR profiles of samples calcined at 600 °C: $LaCoO_3$ (a), $LaCo_{0.8}O_3$ (b), and samples calcined at 900 °C: $LaCoO_3$ (c), $LaCo_{0.8}O_3$ (d), $La_{0.8}CoO_3$ (e), $LaCo_{0.8}Fe_{0.2}O_3$ (f), $La_{0.9}Co_{0.8}Fe_{0.2}O_3$ (g), $La_{0.8}Co_{0.8}Fe_{0.2}O_3$ (h) and $LaFeO_3$ (i). H/Co or H/Co+Fe atomic ratio calculated from H_2 consumption and Co, Fe loadings.

structure up to 600 °C and then partial segregation of Co_3O_4 at 800 °C. Surface compositions as well as oxidation states of elements have been investigated by X-ray photoelectron spectroscopy. The detail of XPS photopeaks are presented in the supporting information which can be downloaded. XPS spectra confirm the theoretical oxidation state of La^{3+}, Co^{3+} as well as lattice oxygen O^{2-} from $LaCoO_3$. Contributions from hydroxyl groups and carbonate species which can be formed after storage in air are also clearly evidenced.

3.4. Surface and bulk properties of non stoichiometric $La_{1-x}CoO_3$ and $LaCo_{1-y}O_3$ solids

Two series of perovskite-based solids were synthesised with a non-stoichiometry on either A-site (*i.e.* $La_{1-x}CoO_3$) or B-site (*i.e.* $LaCo_{1-y}O_3$) and then calcined at either 600 °C or 900 °C. XRD patterns clearly underline that perovskite structure is the main crystalline phase whatever the deficiency on A or B element as compared to the stoichiometric $LaCoO_3$ reference (Fig. 4).

After calcination of $La_{0.8}CoO_3$ at 900 °C, bulk Co_3O_4 species are detected coexisting with the rhombohedral $LaCoO_3$ perovskite structure as reported elsewhere [25]. On the contrary, a slight segregation of La_2O_3 characterised by X-ray lines at $2\theta = 26.1$, 29.0 and 29.9° is shown on $LaCo_{0.8}O_3$ solid after calcination at 600 °C which intensifies on $LaCo_{0.6}O_3$. It is noteworthy that this tendency for La_2O_3 segregation is even more marked after calcination at 900 °C as shown in Fig. 4B (XRD pattern b). Similar tendencies previously established on stoichiometric samples characterize A- and B-deficient perovskites with a strong detrimental effect of the calcination temperature on the specific surface area ascribed to a significant crystallite growth. Agglomeration processes prevail during ageing under reactive atmosphere at 900 °C particularly on $LaCo_{0.8}O_3$. In that case the comparison of the S_{th}/S_{BET} ratio and crystallite size suggests that the loss of specific surface area is not only provoked by a densification of the perovskite crystallites. In fact, the influence of segregated phase such as La_2O_3 is not taken into account in the geometrical model for S_{th} calculation. As a matter of fact, partial segregation of monometallic oxides out of the perovskite structure strongly influences the specific surface area S_{BET} (Table 2). A subsequent increase of the specific surface area of $LaCo_{1-y}O_3$ series calcined at 600 °C suggests that La_2O_3 segregation mainly contributes to the continuous development of the surface up to 21.2 m^2/g. Clearly, the extraction of oxidic La species and further segregation of La_2O_3 outside the rhombohedral perovskite is accentuated after calcination at 900 °C. Moreover it is essentially responsible of the quite high value of specific surface area of 11.9 m^2/g obtained for $LaCo_{0.8}O_3$ even if La_2O_3 is not the main crystalline phase.

H_2-TPR curves recorded on non stoichiometric samples are reported in Fig. 5. As compared to $LaCoO_3$, the reduction processes on $LaCo_{0.8}O_3$ are delayed to higher temperatures on the calcined samples at 600 °C (see Fig. 5b). The decrease in reducibility can be explained from excess lanthanum which likely agglomerates at the surface and then limits the accessibility to perovskite surface. On the other hand, the H_2-TPR profile of non-stoichiometric $LaCo_{0.8}O_3$ perovskite calcined at 900 °C is similar to the stoichiometric one with comparable values for the atomic H/Co ratio. This is in agreement with the cobalt content and a successive two-step reduction processes of Co^{3+} to Co^{2+} and then to Co^0 for $LaCo_{0.8}O_3$.

A different behaviour is observed on $La_{0.8}CoO_3$ calcined at 900 °C with the presence of two distinct peaks at low temperature and a relative increase in intensity of the lowest temperature H_2 uptake (Fig. 5e). This could reflect an enhancement of the Co_3O_4 segregation which is more reducible than Co species from perovskite lattice. The complete reduction of Co_3O_4 into Co^0 proceeds at low temperature starting at 350 °C (with theoretical H/Co = 0.53) with two reduction peaks according to the literature [26]. Such behaviour can explain the higher H/Co value observed at low temperature. The partial reduction of Co^{3+} inside the perovskite structure into Co^{2+} (with theoretical H/Co = 0.8) is observed afterwards. Further reduction of Co^{2+} to Co^0 (H/Co = 1.62) at high temperature also exhibits a complex feature with the presence of a shoulder near 550 °C and a main peak at 620 °C. The formation of cobalt or lanthanum oxide segregated at the surface of perovskite which was previously evidenced leads to a decrease of catalytic performances.

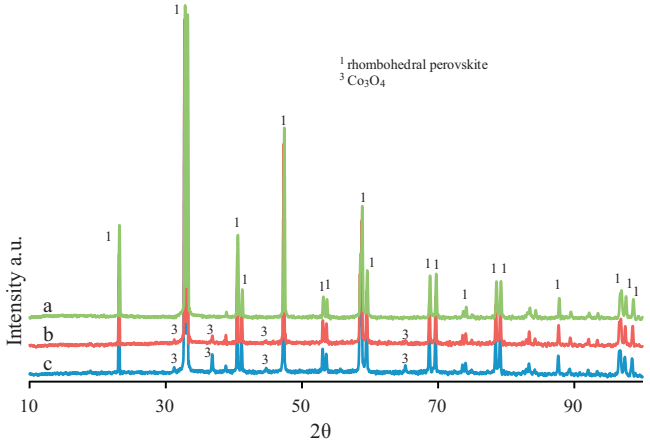

Fig. 6. XRD pattern of $LaCo_{0.8}Fe_{0.2}O_3$ (a), $La_{0.9}Co_{0.8}Fe_{0.2}O_3$ (b) and $La_{0.8}Co_{0.8}Fe_{0.2}O_3$ (c) samples after calcination at 900 °C.

Despite the typical spectral features related to the perovskite systems (see supporting information), excess of lanthanum on $LaCo_{1-y}O_3$ samples leads to an extensive formation of carbonates at the surface as revealed by XPS. On the other hand, the formation of carbonate is strongly attenuated on $La_{0.8}CoO_3$ catalyst. The occurrence of carbonate species accumulated at the surface could limit the accessibility of active sites or limit the oxygen mobility. In the series of $La_{1-x}Co_{1-y}O_3$ catalysts, $LaCo_{0.8}O_3$ which presented a higher carbonate related signal also exhibits poorest catalytic performances after calcination.

3.5. Surface and bulk properties of stoichiometric and non stoichiometric $La_{1-x}Co_{0.8}Fe_{0.2}O_3$ solids

As found, sintering processes usually arise during thermal treatments at high temperature on calcined samples at 900 °C and particularly under reaction conditions in wet conditions. Such trends earlier evidenced [11,27,28] induce a significant loss of specific surface area which can be equally explained on the basis of our results by a crystallite growth and agglomeration processes due to partial extraction of monometallic Co and/or La respectively on A and B-deficient perovskites. It was found that those phenomena alter the reducibility in connection to oxygen mobility. Subsequent incorporation of iron in $LaCoO_3$ based perovskite has been earlier investigated essentially for combustion applications [11] and for the Fischer–Tropsch synthesis [29]. Partial substitution of perovskite would enhance the formation of anionic vacancies and unusual oxidation state for the cations located in the B-site [30]. Hence, in order to improve the resistance of the perovskite towards sintering processes, the partial substitution of cobalt by iron has been investigated with the synthesis of $LaCo_{0.8}Fe_{0.2}O_3$ solid. A solid solution is obtained for $LaCo_{0.8}Fe_{0.2}O_3$ with a rhombohedral perovskite structure (Fig. 6). Similar specific surface area with that of $LaCoO_3$ is also obtained (Table 2). The progressive decrease in lanthanum content in Fe-modified perovskite induces a segregation of cobalt oxide Co_3O_4 and a correlative decrease in specific surface area. Let us note that Fe incorporation has no significant effect

on the crystallite growth which does not vary significantly. On the other hand, it is worthwhile to note that further densification proceeds more significantly on non-stoichiometric $La_{0.8}Co_{0.8}Fe_{0.2}O_3$ perovskite. Hence, more extensive extraction of Co_3O_4 is likely responsible of the gradual decrease of the specific surface area.

The reducibility of this series of catalysts is compared by using H_2-temperature-programmed reduction (Fig. 5). The reduction of Co^{3+} into Co^{2+} is also observed at low temperature after the addition of iron. However the reduction of Co^{2+} into Co^0 becomes strongly delayed at high temperature, thus underlining the stabilisation of the perovskite structure in the presence of iron. The reducibility is not significantly affected by the lanthanum's non-stoichiometry. Atomic H/(Co + Fe) ratio are in agreement with the overall reduction of oxidic cobalt and iron species into Co^0 and Fe^0 respectively during H_2-TPR. This observation emphasises a strong enhancement of the reducibility of iron after Co incorporation as compared to the H_2-TPR curve recorded on $LaFeO_3$ (Fig. 5i). In this latter case no significant H_2 uptake is discernible. Such tendencies have been reported elsewhere [11,31] showing only the reduction of Fe^{4+} to Fe^{3+} at moderate temperature that would correspond to free iron oxide outside the perovskite structure. We did not observe the segregation of bulk detectable oxidic iron species which could be observed on highly Fe loaded perovskite exhibiting an orthorhombic structure. The atomic H/Co ratio observed at low temperature on $La_{0.9}Co_{0.8}Fe_{0.2}O_3$ is in agreement with the complete reduction of Co^{3+} to Co^0 from Co_3O_4 and Co^{3+} to Co^{2+} from perovskite (theoretical value H/Co = 0.97). At higher temperature, the atomic H/Co ratio corresponds to the reduction of Co^{2+} to Co^0 and Fe^{3+} to Fe^0 from perovskite (theoretical value H/(Co + Fe) = 2.0).

Oxidation states of elements of $La_{1-x}Co_{0.8}Fe_{0.2}O_3$ catalysts obtained from XPS measurements are in agreement with the perovskite structure and the progressive formation of Co^{2+} from Co_3O_4 segregation. The most important information is related to the progressive decrease of carbonate species content as the lanthanum content in the formulation decreases.

3.6. Characterisation of aged catalysts

In order to explain surface reconstructions that might occur during ageing under reactive conditions, bulk and surface characterisation were achieved on aged samples. First aspect which can involve deactivation is related to the sintering of solid generally associated with decrease of specific surface area as earlier discussed. The presence of water is found as outstanding parameter in determining the extent of surface reconstruction taking place at 900 °C under reactive conditions. Characterisation of aged catalysts confirms strong decrease of specific surface area after catalytic measurements of $LaCoO_3$, $La_{0.8}CoO_3$ and $LaCo_{0.8}O_3$ solids. The most important decrease arises for $LaCo_{0.8}O_3$. XRD pattern of aged $LaCo_{0.8}O_3$ catalyst puts into evidence the transformation of segregated La_2O_3 into $La(OH)_3$ (Fig. 7) accompanied by an increase in the crystallite size from 34.1 to 44.2 nm. The comparison of the ratio S_{th}/S_{BET} also reveals a more extensive agglomeration lowering the accessible surface. A correlative decrease in the oxygen mobility could explain comparable intrinsic activities recorded on aged $LaCo_{0.8}O_3$ and $LaCoO_3$. This is in agreement with the decrease of specific surface area associated to the disappearance of the La_2O_3 phase. The decrease of specific surface area is slightly limited for the other solids. The highest values (2.8 m^2/g and 2.7 m^2/g) observed for stoichiometric $LaCoO_3$ and $LaCo_{0.8}Fe_{0.2}O_3$ respectively cannot explain the catalytic activity suggested from the evolution of specific and intrinsic activities on aged samples (Table 1).

Thermal treatment under reaction conditions with steam demonstrates the importance of the stabilisation of the catalyst to its definitive arrangement. This resulted in a "positive ageing" which was previously evidenced for combustion reactions [11].

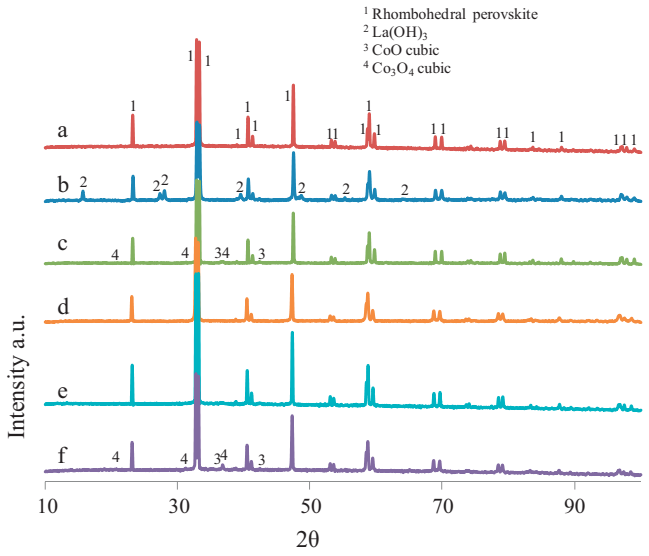

Fig. 7. XRD pattern of $LaCoO_3$ (a), $LaCo_{0.8}O_3$ (b), $La_{0.8}CoO_3$ (c), $LaCo_{0.8}Fe_{0.2}O_3$ (d), $La_{0.9}Co_{0.8}Fe_{0.2}O_3$ (e) and $La_{0.8}Co_{0.8}Fe_{0.2}O_3$ (f) catalysts calcined at 900 °C after the catalytic measurements.

After ageing, higher reaction rates were observed at 575 °C for non-stoichiometric $La_{0.8}CoO_3$ and $La_{0.9}Co_{0.8}Fe_{0.2}O_3$ solids despite their lower specific surface areas as compared to the corresponding stoichiometric catalysts (Tables 1 and 2). Aged $LaCo_{0.8}Fe_{0.2}O_3$ catalyst exhibits typical rhombohedral perovskite structure without any detectable segregation (Fig. 7 XRD pattern (d)). Surprisingly the partial segregation of Co_3O_4 previously observed on $La_{0.9}Co_{0.8}Fe_{0.2}O_3$ is no longer detected after ageing. This suggests the occurrence of reverse process with partial incorporation of segregated cobalt oxide taking place in wet atmosphere in the presence of 15 vol% H_2O. This observation points out the beneficial effect of water with reconstruction more readily between Co_3O_4 and $La(OH)_3$ rather than La_2O_3. The reconstruction of stoichiometric perovskite in lean conditions was previously underlined by several authors [12,32]. The insertion of cobalt in the framework of perovskite at high temperature in the presence of steam could suggest that lanthanum should not be present in stoichiometric amount. On the other hand in stoichiometric compositions, the occurrence of surface enrichment with lanthanum could inhibit the intrinsic activity of perovskite even if the apparent specific surface area appears higher due to lanthanum excess at the surface.

XPS spectral features of stoichiometric $LaCoO_3$ remained unchanged, as compared to calcined ones, except for La 3d, O 1s and N 1s photopeaks. Nitrate and nitrite adsorbed species are stabilised at the surface of catalyst during reaction or during the cooling. Most significant changes on non-stoichiometric aged $LaCo_{0.8}O_3$ catalyst are related to the formation of $La(OH)_3$ previously identified on XRD pattern. Other changes are connected to the decrease of carbonate surface species and the important increase of nitrate species at the surface of the catalyst. Similarly to $LaCo_{0.8}O_3$, nitrate adsorbed species accumulated at the surface of $La_{0.8}CoO_3$ catalyst after ageing.

The Co/La atomic ratio less than 1 (Table 3) clearly highlights a surface enrichment in lanthanum. This can inhibit the catalytic activity after ageing since La_2O_3 can be hydrolysed in presence of high amounts of steam. Highest Co/La as well as N/La atomic ratios are obtained on aged $La_{0.8}CoO_3$. Clearly, these values are much higher than for the stoichiometric $LaCoO_3$ catalyst.

Despite the main contribution from Co^{3+} in $LaCo_{0.8}Fe_{0.2}O_3$, the occurrence of contribution from Co^{2+} is highlighted on

Table 3
XPS measurements of $La_{1-x}CoO_3$, $LaCo_{1-y}O_3$, and $La_{1-x}Co_{0.8}Fe_{0.2}O_3$ solids.

Theoretical composition	$T_{calcination}$/°C	Surface atomic ratio[a]							
		Calcined				After catalytic measurements			
		Co/La[b]	Fe/La[b]	O/La	N/La	Co/La[b]	Fe/La[b]	O/La	N/La
$LaCoO_3$	900 °C	0.50	–	3.11	–	0.30	–	3.12	0.08
$LaCo_{0.8}O_3$	900 °C	0.29	–	2.83	–	0.55	–	4.72	0.69
$La_{0.8}CoO_3$	900 °C	0.90	–	3.06	–	0.89	–	5.93	1.19
$LaCo_{0.8}Fe_{0.2}O_3$	900 °C	0.56	0.10	3.46	–	0.83	0.12	5.40	0.39
$La_{0.9}Co_{0.8}Fe_{0.2}O_3$	900 °C	0.67	0.12	3.55	–	0.79	0.14	5.67	0.79
$La_{0.8}Co_{0.8}Fe_{0.2}O_3$	900 °C	0.78	0.14	4.07	–	0.54	0.16	4.37	0.52

[a] Accuracy ~20%.
[b] Atomic ratio calculated after subtraction of Co and Fe Auger contribution.

aged $La_{0.9}Co_{0.8}Fe_{0.2}O_3$ and $La_{0.8}Co_{0.8}Fe_{0.2}O_3$. Nitrate and nitrite adsorbed species are also detected after ageing.

Quantitative information for aged catalysts is collected in Table 3. The cobalt and iron surface concentration is enhanced on aged $LaCo_{0.8}Fe_{0.2}O_3$. Surface reconstruction is also put into evidence with the increase of Co/La and Fe/La atomic ratios after ageing on $La_{0.9}Co_{0.8}Fe_{0.2}O_3$. This is in agreement with previous XRD patterns which suggested surface reconstructions occurring during thermal ageing on $La_{0.9}Co_{0.8}Fe_{0.2}O_3$ solid.

Most active catalyst after ageing procedure ($La_{0.9}Co_{0.8}Fe_{0.2}O_3$) exhibited intermediate surface Co and Fe concentrations and highest amount of adsorbed nitrate/nitrite species.

3.7. Nature of active sites for N_2O catalytic decomposition on perovskite

In the present study, we observed that N_2O decomposition at high temperature is sensible to the composition of the surface. Several mechanisms are proposed in the literature for the catalytic decomposition of N_2O at medium or high temperature on oxide catalysts [19,33,34]. The interaction of N_2O with the active sites, followed by its dissociation gives rise to N_2 molecule and surface oxygen. The recombination of surface oxygen to gaseous oxygen is generally considered as rate determining step of the reaction mechanism. The nature of active site depends on the nature of the catalyst and the range of temperature. The occurrence of cationic mechanism involving Co^{3+}/Co^{2+} redox system should be strongly related to the surface concentration and the chemical environment of cobalt species [33]. After calcination the surface atomic ratios Co/La are respectively 0.50 and 0.45 for $LaCoO_3$ and $LaCo_{0.8}Fe_{0.2}O_3$. This is in agreement with the lower cobalt loading on $LaCo_{0.8}Fe_{0.2}O_3$. However, higher specific rates are observed on partly substituted perovskite catalyst (Table 1). Clearly, this present study exemplifies the absence of direct relation between cobalt surface concentrations and catalytic performances due to the fact that several types of surface cobalt and lanthanum species are evidenced in the present study. During cooling after the second catalytic test, the formation of nitrate/nitrite is evidenced with XPS measurements. In fact nitrate and nitrite species can be considered as indirect probe molecules that reveal the presence of accessible Co^{3+} at the surface. Above 600 °C, such ad-NO_x species desorb and minimize inhibiting effects on the rate of N_2O decomposition that usually takes place at lower temperature. Highest values for the surface atomic ratio N/La are obtained for aged $La_{0.8}CoO_3$ and $La_{0.9}Co_{0.8}Fe_{0.2}O_3$. These values are in agreement with the lower enrichment in lanthanum for the non-stoichiometric samples.

Another remark concerns the influence of specific surface area that is also not directly related to the catalytic activity. For example, non stoichiometric $La_{0.8}CoO_3$ exhibits lower specific surface area than $LaCoO_3$ after ageing but higher specific reaction rate. Similar trend can be obtained for $La_{0.9}Co_{0.8}Fe_{0.2}O_3$ *versus* $LaCo_{0.8}Fe_{0.2}O_3$. Lanthanum enrichment is responsible for the lower reaction rates on stoichiometric samples.

The following remarks suggest the involvement of oxygen atom as O_2^- or O_2^{2-} [35] which can interact with N_2O for the catalytic decomposition of N_2O at high temperature on perovskite-based materials. The O_2 desorption through recombination of surface peroxide ions (O_2^{2-}) or oxygen ion (O_2^-) can limit the reaction at high temperature. The optimisation of oxygen mobility can be a key point for further improvements of catalytic performances related to perovskite.

The partial substitution of lanthanum by cerium ($La_{0.8}Ce_{0.2}CoO_3$) proposed by Johnson Matthey company [36] is an alternative solution in order to promote catalytic activity. The combination of cerium substitution and optimisation of surface lanthanum concentration proposed in present study can lead to improved catalytic performances as well as thermal stability. The deposition of perovskite onto solids with higher specific surface area than perovskite themselves can also be an alternative strategy for nitric acid plants applications. Higher thermal stability of modified perovskite can also be implemented for N_2O abatement technology in flue-gases of fluidised-bed combustors as alternative candidate of steam-activated FeZSM-5 zeolite which exhibits interesting catalytic activity [37].

4. Conclusion

Three series of catalyst based on perovskite structure were investigated for the catalytic decomposition of N_2O in the presence of 5% NO, 6% O_2 and 15% H_2O at high temperature (850–900 °C). A special attention was paid to the consequences of non-stoichiometric synthesis with stoichiometric $LaCoO_3$ and $LaCo_{0.8}Fe_{0.2}O_3$ as references. After calcination, stoichiometric $LaCoO_3$ and $LaCo_{0.8}Fe_{0.2}O_3$ exhibited highest reaction rates. The lowest reaction rates measured on non-stoichiometric freshly calcined solids for the N_2O decomposition were related to the preferential segregation of Co_3O_4 for $La_{1-x}CoO_3$ and $La_{1-x}Co_{0.8}Fe_{0.2}O_3$ catalysts or La_2O_3 for $LaCo_{1-y}O_3$ catalysts. Accumulation of carbonate species at the surface of catalyst could also have limited the accessibility to the active site.

Overnight ageing led to detrimental effect on catalytic performances which was related to the modification of the surface of perovskite in the presence of water.

Furthermore, the extent of deactivation was significantly decreased on non-stoichiometric $La_{0.9}Co_{0.8}Fe_{0.2}O_3$ after overnight ageing or long term ageing procedure as compared to the stoichiometric $LaCo_{0.8}Fe_{0.2}O_3$ sample. Among the series of catalysts investigated in this study, the reaction rates of $La_{0.8}CoO_3$ and $La_{0.9}Co_{0.8}Fe_{0.2}O_3$ were found to be the highest after ageing procedure. The surface enrichment in lanthanum led to detrimental effect on catalytic performances which was minimised on

non-stoichiometric catalysts. The optimisation of oxygen mobility could improve the catalytic performances.

Acknowledgements

We gratefully acknowledge the Institut de Recherche en Environnement Industriel and the ADEME for a PhD fellowship (Y. Wu). The laboratory participates in the Institut de Recherche en ENvironnement Industriel (IRENI) which is financed by the Communauté Urbaine de Dunkerque, the Région Nord Pas-de-Calais, the Ministère de l'Enseignement Supérieur et de la Recherche, the CNRS and European Fund for Regional Development (FEDER).

We also acknowledge Olivier Gardoll and Laurence Burylo for H_2-TPR, and XRD measurements respectively. We also acknowledge Martine Trentesaux and Dr Anne-Sophie Mamede for fruitful discussions dealing with XPS measurements and Pr R.N. Vannier for XRD refinements.

Appendix A. Supplementary data

Supplementary data associated with this article can be found, in the online version, at http://dx.doi.org/10.1016/j.apcatb.2012.05.033.

References

[1] J. Pérez-Ramirez, F. Kapteijn, K. Schoffel, J.A. Moulijn, Applied Catalysis B 44 (2003) 117.
[2] P. Granger, V.I. Parvulescu, Chemical Reviews 111 (2011) 3155.
[3] P. Granger, P. Esteves, S. Kieger, L. Navascues, G. Leclercq, Applied Catalysis B 62 (2006) 236.
[4] P. Esteves, Y. Wu, C. Dujardin, M.K. Dongare, P. Granger, Catalysis Today 176 (2011) 433.
[5] S. Alini, F. Basile, S. Blasioli, C. Rinaldi, A. Vaccari, Applied Catalysis B 70 (2007) 323.
[6] J. Pérez-Ramirez, M. Santiago, Chemical Communications (2007) 619.
[7] G. Giecko, T. Borowiecki, W. Gac, J. Kruk, Catalysis Today 137 (2008) 403.
[8] M. Ruszak, M. Inger, S. Witkowski, M. Wilk, A. Kotarba, Z. Sokja, Catalysis Letters 126 (2008) 72.
[9] J.P. Dacquin, C. Lancelot, C. Dujardin, P. Da Costa, G. Djega-Mariadassou, P. Beaunier, S. Kaliaguine, S. Vaudreuil, S. Royer, P. Granger, Applied Catalysis B 91 (2009) 596.
[10] C. Dujardin, I. Twagirashema, P. Granger, Journal of Physical Chemistry C 112 (2008) 17183.
[11] N.A. Merino, B.P. Barbero, P. Ruiz, L.E. Cadús, Journal of Catalysis 240 (2006) 245.
[12] I. Twagirashema, M. Engelmann-Pirez, M. Frere, L. Burylo, L. Gengembre, C. Dujardin, P. Granger, Catalysis Today 119 (2007) 100.
[13] J. Rodriguez-Carjaval, Physica B 192 (1993) 55;
J. Rodríguez-Carvajal, Commission on Powder Diffraction (IUCr) Newsletter, 26, 2001, pp. 12–19.
[14] D.A. Shirley, Physical Review B 5 (1972) 4709.
[15] J.P. Dacquin, C. Dujardin, P. Granger, Catalysis Today 137 (2008) 390.
[16] P. Trambouze, H. Van Landeghem, J.P. Wauquier, Les Réacteurs Chimiques, Conception, Calcul, Mise en Oeuvre, Technip, Paris, 1984.
[17] C.G.S. Pillai, A.M. George, International Journal of Thermophysics 4 (2) (1983) 183–188.
[18] J.F. Lepage, J. Cosyns, P. Courty, E. Freund, J.P. Franck, Y. Yacquin, B. Juquin, C. Marsilly, G. Martino, J. Miquel, R. Montarnal, A. Sugier, H. Van Landeghem, Catalyse de Contact, Technip, Paris, 1978, 53.
[19] F. Kapteijn, J. Rodriguez-Mirasol, J.A. Moulijn, Applied Catalysis B 9 (1996) 25.
[20] E.V. Kondratenko, V.A. Kondratenko, M. Santiago, J. Perez-Ramirez, Applied Catalysis B 99 (2010) 66.
[21] F.J. Perez-Alonso, I. Melián-Cabrera, M. López Granados, F. Kapteijn, J.L.G. Fierro, Journal of Catalysis 239 (2006) 340.
[22] J.P. Dacquin, C. Dujardin, P. Granger, Journal of Catalysis 253 (2008) 37.
[23] S. Royer, D. Duprez, S. Kaliaguine, Journal of Catalysis 234 (2005) 364.
[24] S. Royer, F. Bérubé, S. Kaliaguine, Applied Catalysis A 282 (2005) 273.
[25] G.L. Chiarello, J.-D. Grunwaldt, D. Ferri, F. Krumeich, C. Oliva, L. Forni, A. Baiker, Journal of Catalysis 252 (2007) 127.
[26] M.M. Yung, E.M. Holmgreen, U.S. Ozkan, Journal of Catalysis 247 (2007) 356.
[27] C. Batiot-Dupeyrat, F. Martinez-Ortega, M. Ganne, J.M. Tatibouët, Applied Catalysis A 206 (2001) 205.
[28] M.F.M. Zwinkels, S. Druesne, E. Björnbom, P.G. Menon, S.G. Järås, Industrial and Engineering Chemistry Research 37 (1998) 391.
[29] L. Bedel, A.-C. Roger, J.-L. Rehspringer, Y. Zimmermann, A. Kiennemann, Journal of Catalysis 235 (2005) 279.
[30] H. Dai, H. He, P. Li, L. Gao, C. Au, Catalysis Today 90 (2004) 231.
[31] P. Ciambelli, S. Cimino, L. Lisi, M. Faticanti, G. Minelli, I. Pettiti, P. Porta, Applied Catalysis B 33 (2001) 193.
[32] H. Tanaka, M. Uenishi, M. Taniguchi, I. Tan, K. Narita, M. Kimura, K. Kaneko, Y. Nishihata, J. Mizuki, Catalysis Today 117 (2006) 321.
[33] P. Pietrzyk, F. Zasada, W. Piskorz, A. Kotarba, Z. Sojka, Catalysis Today 119 (2007) 219.
[34] L. Obalova, V. Fila, Applied Catalysis B 70 (2007) 353.
[35] M. Nakamura, H. Mitsuhashi, N. Takezawa, Journal of Catalysis 138 (1992) 686.
[36] S.A. Axon, D.R. Coupland, J.R. Foy, J. Ridland, I.C. Wishart, International Patent WO 2004/096703 A2 (2004).
[37] M. Santiago, M.A.G. Hevia, J. Pérez-Ramirez, Applied Catalysis B 90 (2009) 83.